

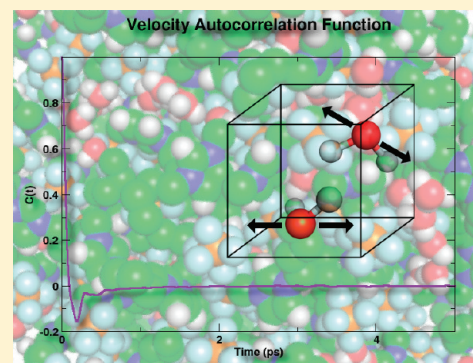
# Molecular Dynamics Simulation of the Structure and Dynamics of Water–1-Alkyl-3-methylimidazolium Ionic Liquid Mixtures

Trinidad Méndez-Morales,<sup>†</sup> Jesús Carrete,<sup>†</sup> Óscar Cabeza,<sup>‡</sup> Luis J. Gallego,<sup>†</sup> and Luis M. Varela<sup>\*,†</sup>

<sup>†</sup>Grupo de Nanomateriales y Materia Blanda, Departamento de Física de la Materia Condensada, Universidad de Santiago de Compostela, E-15782 Santiago de Compostela, Spain

<sup>‡</sup>Facultad de Ciencias, Universidade de A Coruña, Campus A Zapateira s/n, E-15008, A Coruña, Spain

**ABSTRACT:** We have performed extensive molecular dynamic simulations to analyze the influence of cation and anion natures, and of water concentration, on the structure and dynamics of water–1-alkyl-3-methylimidazolium ionic liquid mixtures. The dependence on water concentration of the radial distribution functions, coordination numbers, and hydrogen bonding degree between the different species has been systematically analyzed for different lengths of the cation alkyl chain (alkyl = ethyl, butyl, hexyl, and octyl) and several counterions. These include two halogens of different sizes and positions in Hoffmeister series,  $\text{Cl}^-$  and  $\text{Br}^-$ , and the highly hydrophobic inorganic anion  $\text{PF}_6^-$  throughout its whole solubility regime. The formation of water clusters in the mixture has been verified, and the influences of both anion hydrophobicity and cation chain length on the structure and size of these clusters have been analyzed. The water cluster size is shown to be relatively independent of the cation chain length, but strongly dependent on the hydrophobicity of the anion, which also determines critically the network formation of water and therefore the miscibility of the ionic liquid. The greater influence of the anion relative to the cation one is seen to be reflected in all the analyzed physical properties. Finally, single-particle dynamics in IL–water mixtures is considered, obtaining the self-diffusion coefficients and the velocity autocorrelation functions of water molecules in the mixture, and analyzing the effect of cation, anion, and water concentration on the duration of the ballistic regime and on the time of transition to the diffusive regime. Complex non-Markovian behavior was detected at intermediate times within an interval progressively shorter as water concentration increases.



## 1. INTRODUCTION

Pure ionic liquids (ILs) are nonaqueous but polar solvents that have attracted enormous research effort for both theoretical reasons and with a view to their potential applications. Many are the properties which confer ILs their unique character as alternative green solvents: high cohesive energy densities combined with melting points often below 100 °C,<sup>1,2</sup> nonvolatility, nonflammability, high thermal and electrochemical stability, ability to dissolve an enormous range of inorganic, organic, and polymeric materials at very high concentrations, noncorrosiveness, low viscosity, negligible vapor pressure, and so forth.<sup>3–7</sup> These systems (whose number has been evaluated to be around 10<sup>18</sup>) are considered to be tunable “designer” solvents, since a wide variation in physicochemical properties such as viscosity, catalytic activity, or solvation can be obtained by changing the anion or the lateral chains attached to the heterocyclic unit.

The mixing of ILs with both inorganic and organic compounds, particularly water, is extremely important in many of their applications. For example, the immiscibility of ILs with organic compounds is used in biphasic catalysis, and in some reactions IL/water mixtures are employed as biphasic systems. The presence of water in ILs is almost inevitable,<sup>8,9</sup> and its well-known influence on the nanostructural organization of room-temperature molten salts is a central topic in synthetic chemistry and catalysis. Many

experimental studies have been performed to adequately characterize the influence of water on IL nanostructure, ranging from small angle neutron scattering (SANS)<sup>10</sup> to surface properties.<sup>11</sup> Turmine et al.<sup>11</sup> verified the existence of a surface transition for aqueous solutions of imidazolium-based ionic liquids associated to the nanoaggregation of electrolytes. Moreover, the spontaneous self-organization and the formation of a liquid-crystalline gel were shown by Firestone and co-workers<sup>12</sup> adding water to 1-decyl-3-methylimidazolium bromide, and Antonietti and co-workers<sup>13</sup> showed that, with the addition of water, ILs exhibit classical surfactant self-organization with high order.

Despite all of these studies, our knowledge of the interaction between water and ILs remains somewhat empirical, as it has been pointed out by Jiang et al.<sup>14</sup> Particularly, the role of cation and anion is not yet fully understood, and its impact on magnitudes such as the hydrogen bonding degree in bulk mixtures or the velocity autocorrelation functions has not been previously considered in literature. Since it is normally very difficult to experimentally probe the properties of ILs at the atomic level, particularly the environment experienced by a solute in an IL,

**Received:** March 22, 2011

**Revised:** April 29, 2011

**Published:** May 11, 2011

and the theoretical studies reported so far on these systems are somehow scarce, computer simulations may play an essential role for understanding their behavior. In fact, several computational studies of the properties of both pure ILs and IL/water mixtures have been reported in the last years, dealing mainly with thermodynamic and structural properties and single particle dynamics (for a recent review, see ref 15 and references therein). However, mixtures have attracted less attention. In what the aqueous mixtures are concerned, Hanke and Lynden-Bell<sup>16</sup> reported a seminal molecular dynamics (MD) study of the structure and physicochemical properties of water–1,3-dialkyl-imidazolium mixtures, providing the first molecular picture for the water structure and water-enhanced ion dynamics in mixtures. Canoniga-Lopes et al.<sup>17</sup> contributed to a new understanding of the solvation mechanisms of nonpolar and polar molecules in ILs reporting the existence of microphase separation of polar and nonpolar domains. Jiang et al.<sup>14</sup> analyzed the effect of varying water concentrations on the nanostructural organization of IL–water mixtures. These authors considered the relative role of hydrophobic and electrostatic interactions in the evolution of the polar and water networks with water content, as well as on the turnover point where ordered micelle (cation–cation) structure and water network are formed. Moreover, Spickermann et al.<sup>18</sup> performed Carr–Parrinello simulations in which they considered the structure of the hydration shells around ion pairs, proving that water–water radial distribution functions (RDFs) differ significantly from bulk water and that no ion pair dissociation takes place since the solvation of both cation and anion is not complete. Recently, Porter et al.<sup>19</sup> considered the size of water clusters in aqueous IL mixtures and proved that they are hydrogen bonded to two anions with the cation playing a minor role.

As it is well-known, the nanostructures of pure ILs and their mixtures are highly dependent on the choice of the cation and anion. Particularly, the length of the chains attached to the heterocyclic unit is conventionally thought to be the main responsible for the hydrophobicity of ILs, and therefore of the properties of their mixtures with water, and the role of the anion is not yet well-understood. An adequate microscopic understanding of the role of both species in the solvation of water and the rest of physicochemical properties in IL–water mixtures is of fundamental importance. However, the role of both cation and anion in the structure and dynamics of ILs and their mixtures has not received attention until recently. For pure ILs, Urahata and Ribeiro<sup>20</sup> reported a systematic analysis of the matter simulating 10 different systems at 323 K using united atom force fields, in which different anion sizes ( $\text{F}^-$ ,  $\text{Cl}^-$ ,  $\text{Br}^-$ , and  $\text{PF}_6^-$ ) and alkyl chain lengths of 1-alkyl-3-methylimidazolium cations (alkyl = methyl, ethyl, butyl, and octyl) were considered. For what mixtures are concerned, Feng and Voth<sup>21</sup> reported very recently the first (to our knowledge) MD analysis of the role of alkyl size chain of both cation and anion on the structure and dynamics of IL/water mixtures. The authors considered three IL/water mixtures at various water mole fractions: 1-butyl-3-methylimidazolium  $\text{BMIMBF}_4^-$ , 1-octyl-3-methylimidazolium  $\text{OMIMBF}_4^-$ , and  $\text{OMIMCl}$ , and they found significant influence of the alkyl chain length on the aggregation behavior of the cation, since the longer the chain the more extensive is micelle formation at large water proportions. On the other hand, water–anion interactions seem to be responsible for the water structure at low water contents. However, to the best of our knowledge, no results have been reported for 1-ethyl-3-methylimidazolium ( $\text{EMIM}^+$ ) or 1-hexyl-3-methylimidazolium ( $\text{HMIM}^+$ ), and no attention

seems to have been devoted to the strongly hydrophobic anion  $\text{PF}_6^-$ , probably due to its very low solubility in water (from  $w = 0$  to  $w \approx 26\%$  and from  $w \approx 99.84\%$  to  $w = 100\%$  in  $\text{BMIMPF}_6^-$ ; from  $w = 0$  to  $w \approx 22\%$  and from  $w \approx 99.95\%$  to  $w = 100\%$  in  $\text{HMIMPF}_6^-$ ; from  $w = 0$  to  $w \approx 20\%$  and from  $w \approx 99.99\%$  to  $w = 100\%$  in  $\text{OMIMPF}_6^-$ ).<sup>22–25</sup> Moreover, the systematic analysis of the influence of both ionic species on the degree of hydrogen bond in the bulk—crucial for understanding the nanostructure of these systems—or in the velocity autocorrelation functions in IL/water mixtures have not been explicitly considered up to now, although they are essential for understanding the solvation mechanisms and dynamics of these systems.

Although MD simulations of transport properties of pure ILs were reported for the first time in the literature at the beginning of this century,<sup>16,20,26</sup> only recently single-particle dynamics in IL–water mixtures has begun to be considered. In particular, Porter et al.<sup>19</sup> performed MD calculations to obtain the diffusion coefficients and the mean square displacement (MSD) of different species in mixtures of a water miscible ( $\text{EMIMBF}_4^-$ ) and a water immiscible ( $\text{EMIMNTf}_2^-$ ,  $\text{NTf}_2^-$  bis(trifluoromethylsulfonyl)imide) IL containing very small amounts of water. These authors reported a wide range of thermodynamic and transport properties of mixtures of  $\text{EMIMEtSO}_4^-$  ( $\text{EtSO}_4^-$ , ethyl sulfate), including rotational relaxation times, self-diffusivity, shear viscosity, and thermal conductivity. More recently, Feng and Voth<sup>21</sup> investigated the concentration dependence of the self-diffusion coefficients of water mixtures of EMIM, BMIM, and OMIM tetrafluoroborates and chlorides, together with the water rotational correlation time in these systems. However, systematic calculations of the velocity autocorrelation functions (VACF) of aqueous mixtures of the first members of the imidazolium family have not been reported yet, nor they have the roles of both ionic species and of water content in the times of transition to both ballistic and diffusive regimes and in the duration of the subdiffusive regime at intermediate times.

In the work described here we performed extensive MD simulations to investigate the structure and some dynamic properties of aqueous mixtures of four members of the family of the 1-alkyl, 3-methylimidazolium (alkyl = ethyl, butyl, hexyl, octyl) (AMIM) for three counterions, with different positions in the Hoffmeister series ( $\text{Br}^-$  and  $\text{Cl}^-$ ) and one hydrophobic ( $\text{PF}_6^-$ ) with low miscibility with water throughout its entire solubility region (see schemes in Figure 1). We analyze the influence of the chemical structure of the IL and of the water concentration on the evolution of the microstructure of the mixtures (radial distribution functions, hydrogen bonding degree, coordination numbers) and on several transport properties like the self-diffusion coefficients and MSDs of water molecules in the mixtures, with an analysis of the ballistic and diffusive regimes, and water–water VACFs.

The remainder of this paper is organized as follows. In section 2 we describe the computational methods employed in this paper; in section 3 we present and discuss the obtained results, and in section 4 we summarize our main conclusions.

## 2. COMPUTATIONAL METHODS

MD simulations for pure AMIM ILs and their mixtures with water were performed using Gromacs package.<sup>27,28</sup> All of the simulations except those for  $\text{EMIMPF}_6^-$  were carried out at 298.15 K, and the water molar percentages in the water–IL

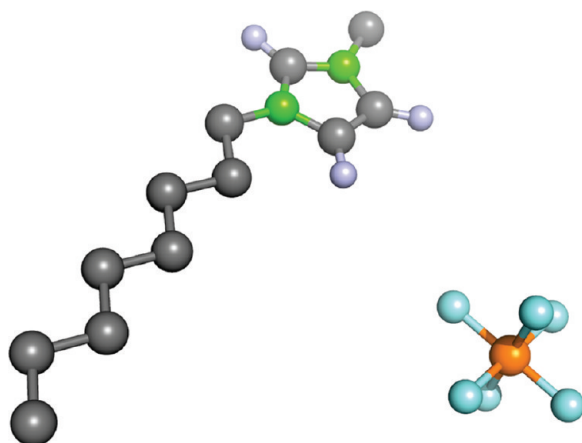


**Figure 1.** Molecular structures of 1-octyl-3-methylimidazolium, and hexafluorophosphate ions.

mixtures were those of the set  $w = \{0, 0.50, 0.95, 5.00, 10.60, 25.00, 50.00, 75.00, 80.00, 85.00, 90.00, 95.00, 99.50, 100.00\% \}$  for which the different ILs are miscible with water. These percentages were calculated fixing the number of ion pairs at 210 (except with 99.50 and 100.00%, which had 50 and none, respectively) and adjusting the number of water molecules in each situation, so they are equivalent to the mole fractions. EMIMPF<sub>6</sub> is solid at ambient temperature, and to our knowledge, the highest melting temperature reported in the literature for EMIMPF<sub>6</sub> is  $T = 333.15 \text{ K}$ ,<sup>25</sup> so we chose  $T = 340.15 \text{ K}$  as the simulation temperature to ensure the substance is in its liquid phase. The simulations for AMIMCl and AMIMBr were carried out only for the two cations with the longest chain, hexyl and octyl, since the other compounds are solid at ambient temperature.

The parametrization of the ions was made in the framework of the GROMOS96 43A1 FF force field:<sup>29</sup>

$$\begin{aligned} V(\mathbf{r}; s) = & \sum_{n=1}^{N_b} \frac{1}{4} K_{b_n} [b_n^2 - b_{0_n}^2]^2 + \sum_{n=1}^{N_\theta} \frac{1}{2} K_{\theta_n} [\cos \theta_n - \cos \theta_{0_n}]^2 \\ & + \sum_{n=1}^{N_\xi} \frac{1}{2} K_{\xi_n} [\xi_n - \xi_{0_n}]^2 + \sum_{n=1}^{N_\phi} K_{\phi_n} [1 + \cos(\delta_n) \cos(m_n \varphi_n)] \\ & + \sum_{i,j} \left( \frac{C12_{ij}}{r_{ij}^{12}} - \frac{C6_{ij}}{r_{ij}^6} \right) + \sum_{i,j} \frac{q_i q_j}{4\pi \epsilon_0 \epsilon_1 r_{ij}} \quad (1) \end{aligned}$$

The first four terms represent the bonded interactions, that is, bonds, angles, and torsions, and the nonbonded interactions are described in the last two terms, including van der Waals and Coulombic interactions.  $b_n$  and  $\theta_n$  are the actual bond between atoms  $i$  and  $j$  and the actual angle between atoms  $i$ ,  $j$ , and  $k$ , respectively. Equilibrium bond lengths,  $r_0$ , and angles,  $\theta_0$ , were obtained from X-ray diffraction, while force constants ( $K_b$ ,  $K_\theta$ ) were taken from experimental spectroscopic data. In the improper and torsional dihedral-angle interaction terms,  $\xi_n$  and  $\varphi_n$  are the actual values of a dihedral angle defined by atoms  $i$ ,  $j$ ,  $k$ , and  $l$ ,  $\delta_n$  is the phase shift (restricted to 0 or  $\pi$ ), and  $m_n$  is the multiplicity of the torsional dihedral angle.  $C12_{ij}$  and  $C6_{ij}$  parameters in the Lennard-Jones (LJ) interactions depend on the atoms involved in the interaction, and they are obtained from parameters for each type of atom using geometric combination rules,  $C12_{ij} = (C12_{ii} \cdot C12_{jj})^{1/2}$  and  $C6_{ij} = (C6_{ii} \cdot C6_{jj})^{1/2}$ . For

these values we used  $C6_{ii} = 4\epsilon_i \sigma_i^6$  ( $\text{kJ} \cdot \text{nm}^6 \cdot \text{mol}^{-1}$ ) and  $C12_{ii} = 4\epsilon_i \sigma_i^{12}$  ( $\text{kJ} \cdot \text{nm}^{12} \cdot \text{mol}^{-1}$ ), where  $\sigma_i$  is the distance at which the LJ potential vanishes for species  $i$ . The electrostatic interactions include parameters defined as the charges on the atoms,  $q_i$ , the dielectric permittivity of vacuum ( $\epsilon_0$ ), and the relative permittivity of the medium in which the atoms are embedded ( $\epsilon_1$ ). The value of  $\epsilon_1$  is conventionally set to 1.

The cations were modeled using a united-atom representation of the CH<sub>2</sub> and CH<sub>3</sub> groups in the alkyl chain, as well as of the methyl group attached to the imidazolium ring. Partial charges were calculated by the ab initio restrained electrostatic potential (RESP) fitting method.<sup>30</sup> In what the anions are concerned, both Br<sup>-</sup> and Cl<sup>-</sup> were modeled by single sites of charge  $-e$ , while PF<sub>6</sub><sup>-</sup> was modeled as a set of seven sites with partial charges of 1.100 for the phosphorus atom and -0.350 for the fluorine atoms. On the other hand, water molecules were described by means of the conventional Berendsen's SPC water model,<sup>31</sup> and the electrostatic interactions were treated using particle-mesh Ewald (PME) method<sup>32,33</sup> with a grid spacing of 0.12 nm and a cubic interpolation. The search for neighbors was made up to a distance of 0.9 nm from the central ion and was actualized every five simulation steps.

The SPC water model is developed in the GROMOS force field. This model considers water as a rigid molecule with an ideal tetrahedral shape which consists of a LJ interaction site with a negative partial charge (-0.82) placed on the oxygen atom and two positive partial charges (+0.41) located at the positions of the hydrogen atoms. Many other models for water were proposed over the years, such as TIP3P<sup>34</sup> or TIPSP<sup>35</sup>. The former model is implemented in the AMBER force field,<sup>36</sup> and it has three interaction points; this model, as the SPC model, shows a stronger interaction of water and ions because of the larger partial charges on the atoms compared to TIPSP water. The TIPSP model was made for the OPLS-AA force field,<sup>37</sup> and in addition to the LJ center placed on the oxygen and the charges located at the hydrogen atoms, it places two partial charges representing the lone pairs of the oxygen atom. However, this latter water model overestimates the density more than a 5% and does not describe some structural properties in the best manner, the SPC model giving more accurate results.<sup>38</sup>

None of these models is able to reproduce the immiscibility of AMIMPF<sub>6</sub> with water, having to use some special techniques to achieve this result.<sup>22,39</sup> As no water model available is able to reproduce all the water properties with good accuracy, our justification for the choice of the SPC water model is that this popular model describes the global structural properties of pure liquid water in a good manner with a low computational cost.

As a check of the computational method employed, Figure 2a shows the comparison between the RDFs of BMIMPF<sub>6</sub> mixed with a 25% of water provided by GROMOS96 and the OPLS-AA force fields, for which the main difference is that the former one is a united-atom representation and the latter one is an all-atom force field. Only the anion-anion RDF exhibits significant differences, showing a double peak in the GROMOS force field and a single peak in the OPLS-AA one. Figure 2b compares the RDF of pure water for the SPC and TIPSP models with the experimental radial distribution function at 298 K.<sup>40</sup> As can be seen, both the SPC and TIPSP models provide a good description of the experimental RDF.

Initial configurations were energy-minimized for 1 000 000 steps using the steepest descent method to remove bad contacts resulting from the initial random configuration of cations

and anions. The maximum step size and the tolerance were 0.01 nm and  $0.1 \text{ kJ} \cdot \text{nm}^{-1} \cdot \text{mol}^{-1}$ , respectively. The equilibration phase was performed in the isothermal–isobaric ensemble during 100 steps to ensure the full equilibration of all the properties of the system. The results of an additional 2000 ps simulation in the isothermal–isobaric ensemble were used for analysis. Temperature control was implemented using a Berendsen thermostat.<sup>41</sup> Cations and anions (and water in cases where we include the solvent) were separated in two (three) baths with temperature coupling constants of 0.1 ps. Pressure control was set by means of a Berendsen barostat<sup>41</sup> with a reference pressure of 1 atm, an isothermal compressibility of  $4.5 \times 10^{-5} \text{ bar}^{-1}$ , and a relaxation time of 1.0 ps.

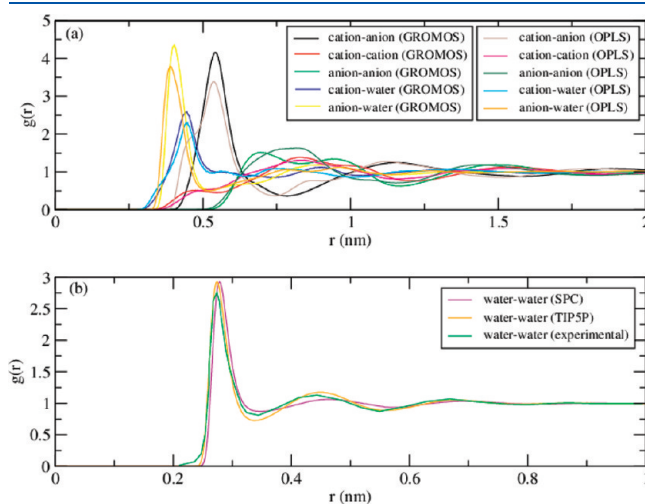


**Figure 2.** (a) Comparison between RDFs of BMIMPF<sub>6</sub> at 25% water concentration calculated using GROMOS and OPLS-AA force fields, and (b) comparison between experimental RDF of pure water with the predictions of SPC and TIPSP models of water, used with the GROMOS and the OPLS-AA force fields, respectively.

These simulations provide us a sequence of configurations, that is, positions and instantaneous velocities of all atoms of the system, which were analyzed to obtain structural, thermodynamic, and dynamical information of the mixed IL–water systems mentioned above.

### 3. RESULTS AND DISCUSSION

The structure of dense fluids is usually characterized by means of the RDF defined as

$$g(r) = \frac{1}{V} \left\langle \sum_{ij} \delta(r - r_{ij}) \right\rangle \quad (2)$$

where  $V$  stands for the system volume,  $i$  and  $j$  run over all the particles, and brackets indicate the ensemble average. Calculated ion–ion RDFs of the pure ILs analyzed in this paper are shown in Figures 3 and 4. All RDFs were calculated using the geometric center of the anions and the geometric center of the imidazole ring of the cations. It is noteworthy that, to the best of our knowledge, this is the first time that the RDFs of pure HMIMPF<sub>6</sub> and OMIMPF<sub>6</sub> are reported at ambient temperature, while the RDF of pure BMIMPF<sub>6</sub> was showed for the first time by Morrow and Maginn.<sup>42</sup> Figure 3 shows the influence of the cationic chain length on the RDFs of the analyzed pure AMIMs, and Figure 4 presents the influence of the anion on the structure of the system for the ILs with a melting temperature below room temperature. As can be seen in these representations, the calculated RDFs exhibit some of the characteristic features previously reported in literature: (i) cation–cation and cation–anion distances around 0.7 and 0.5 nm, respectively, in coincidence with previously reported results (see ref 43 and references therein), (ii) considerably long-ranged out-of-phase distribution of one ion around the other one as is the case for other imidazolium-based ionic liquids containing halides and PF<sub>6</sub><sup>-</sup> anions. This order is preserved typically for at least three interionic distances, thus confirming the so-called pseudolattice arrangement in the liquids, on the basis of the Bahe–Varela model,<sup>44,45</sup> and (iii) very

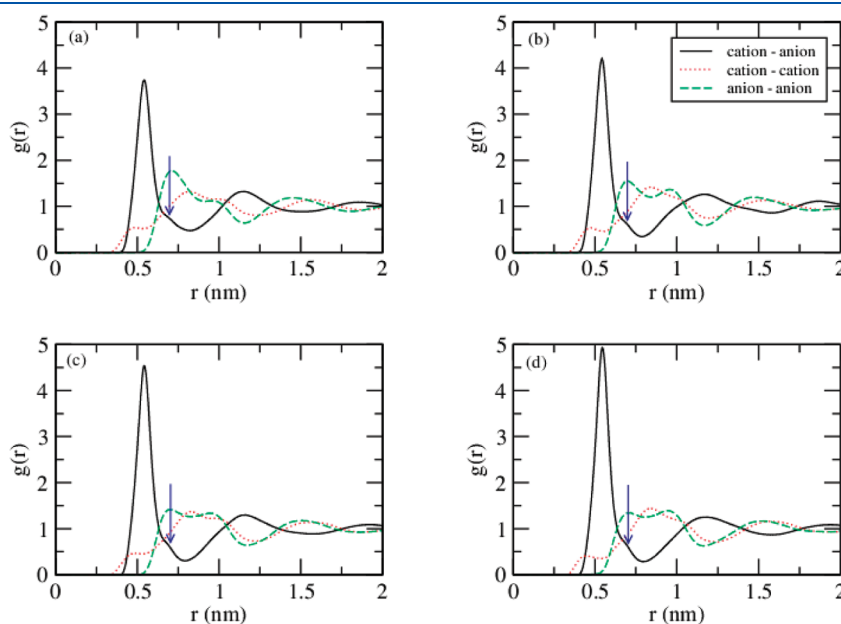


**Figure 3.** RDFs of EMIMPF<sub>6</sub> at 340.15 K (a), BMIMPF<sub>6</sub> (b), HMIMPF<sub>6</sub> (c), and OMIMPF<sub>6</sub> (d) at 298.15 K and 1 atm. The arrows indicate the shoulder in the first peak of the RDF mentioned in the text.

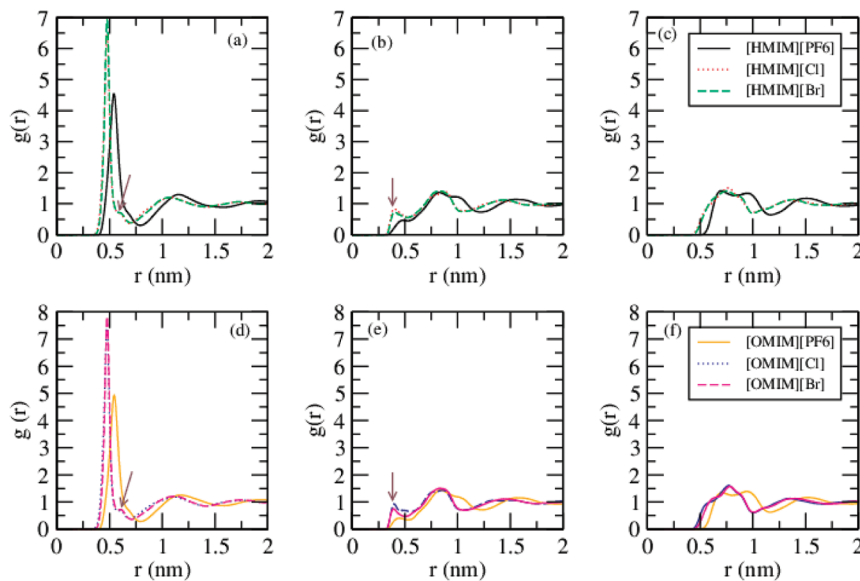


**Figure 4.** RDFs for cation–anion (a, d), cation–cation (b, e), and anion–anion (c, f) of  $\text{HMIM}^+$  and  $\text{OMIM}^+$  for three different counterions ( $\text{PF}_6^-$ ,  $\text{Cl}^-$ , and  $\text{Br}^-$ ) at 298.15 K and 1 atm. The arrows indicate the features of the RDFs mentioned in the text.

limited presence of like-ions in the first coordination shell of ions of the other type. However, we did not obtain the shoulders in the cation–cation RDFs recently reported by Bowron et al.<sup>43</sup> representative of ring stacking; our simulations are more in agreement with those reported by Urahata and Ribeiro,<sup>20</sup> who did not find such a feature. Particularly, it is visible in Figure 3 that the RDFs show considerable clustering of  $\text{PF}_6^-$  anions around the imidazolium cation (at an average distance of 0.54 nm) and ordering up to 2 nm. The most significant effects of the increment of the chain length of the cation on the anion–cation RDF is the increase of the height of the first peak in the cation–anion RDF. Given this peak, we evaluated the coordination numbers integrating numerically the radial distribution function  $4\pi r^2 g(r)$  up to its first minimum. Our calculated coordination number for the cation–anion first peak in pure  $\text{BMIMPF}_6$ , 5.4, differs from another simulation values near 7 reported in the literature,<sup>42</sup> but one must recall that this property is very sensitive to the choice of the position of the minimum. It is also noteworthy that the first peak of the cation–anion RDF exhibits a shoulder around 0.67 nm (see arrows in Figure 3), a feature which has also been observed in some liquids such as Ga, Si, Sn, or Bi (see ref 46 and references therein), and it has been interpreted as a signature of a short-lived diatomic molecular unit. Contrarily to what happens with this first peak, the impact of the variation of the cationic chain length in the distribution of higher order neighbors seems to be relatively limited. On the other hand, a more complex structure is observed in the case of cations, with a weak first peak at 0.48 nm and a double second peak centered at 0.95 nm. This structure is probably associated to the different lengths of the cation alkyl side chains of the  $\text{AMIM}^+$  cations.<sup>19</sup> As can be seen in the representation, a cation–cation RDF is very resilient to the change of the alkyl chain length. Probably, the most notable effect of the modification of the number of carbon atoms in the alkyl side chain of the cation one is the smoothing out of the shoulder appearing in the second peak of the cation–cation RDF at 0.95 nm, what could indicate a more difficult ring-stacking of the cations as their chain length is increased. Concerning the anion network structure, once again

we see that considerable long-range ordering is observed in the anion–anion RDFs and that a double first peak centered at 0.84 nm is obtained for  $\text{PF}_6^-$  anions. The influence of the chain length of the cation is registered mainly on the first peak of the anion–anion RDF. This peak suffers a progressive reduction of its height and an overlapping with the second peak, which is even dominant for  $\text{OMIMPF}_6$ , reflecting a reduction of the ability of  $\text{PF}_6^-$  to coordinate with the cations as the chain length of the latter is increased. In fact, the calculated numbers of anions coordinating our studied cations were 6.87 for  $\text{EMIMPF}_6$ , 5.40 for  $\text{BMIMPF}_6$ , 5.37 for  $\text{HMIMPF}_6$ , and 3.48 for  $\text{OMIMPF}_6$ . Similar trends were observed for the halogenated ILs analyzed in this paper.

The effect of the anion in the RDFs of the different species in our studied ILs can be seen in Figure 4. A first notable effect is that the calculated first peak of the anion–cation RDFs for the  $\text{PF}_6^-$  anion is lower and broader than those obtained for the halogen anions (Figure 4a,d), and it is a little bit displaced to higher distances with respect to its halogen counterparts, probably due to the greater hard sphere radius of the  $\text{PF}_6^-$  anion. The shoulder in the first peak mentioned above is more visible for the halogen anions than for  $\text{PF}_6^-$  (see arrows in Figure 4a,d). Moreover, a first peak around 0.4 nm is registered in the cation–cation RDF for the halogen ions, but it is almost completely smeared out in  $\text{HMIMPF}_6$  and also  $\text{OMIMPF}_6$  (see arrows in Figure 4b,e). The results obtained with this force field are clearly comparable to both experimental and calculated RDFs previously reported in the literature for the same or related ILs (see for example refs 20, 47–51).

Water–water (w/w), water–cation, and water–anion RDFs in mixed systems are represented in Figures 5, 6, and 7, respectively. In the first of these representations, w/w RDF is seen to exhibit a very strong clusterization at the lowest water concentration, as indicated by the height of its first peak. The position of this peak (ca. 0.27 nm) indicates that the water molecules in the first coordination shell are hydrogen bonded according to the criteria given below for this kind of bond to exist ( $r < 0.35$  nm, angle acceptor-H-donor below  $35^\circ$ ). As expected,

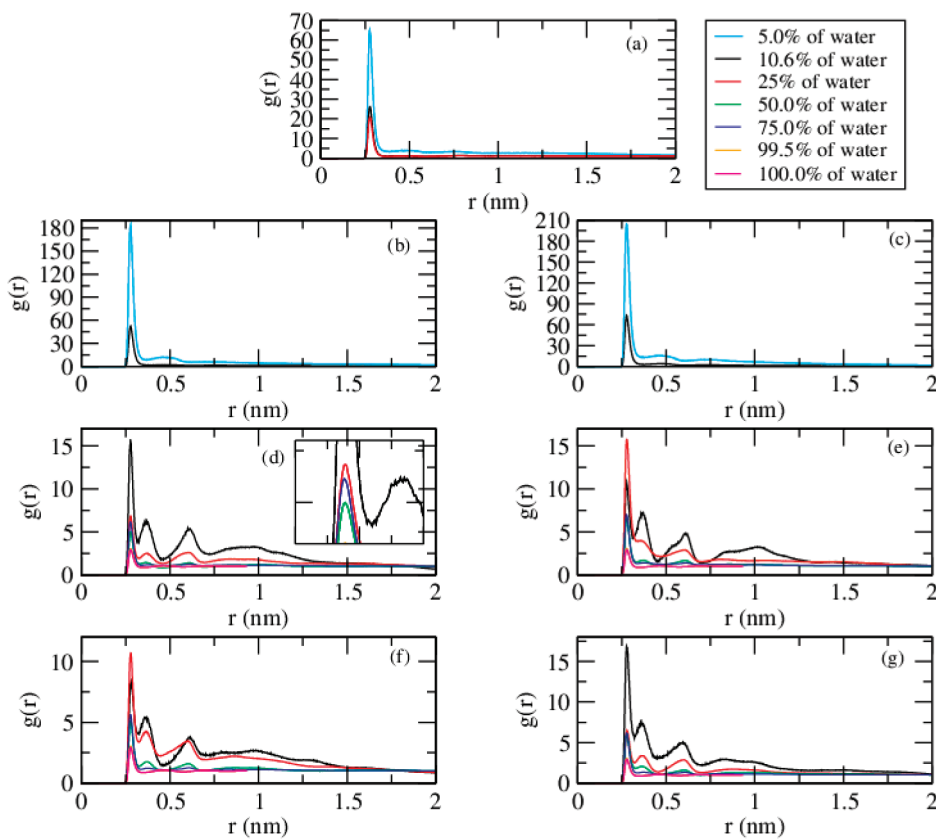


**Figure 5.** Concentration dependence of water–water RDFs for BMIMPF<sub>6</sub> (a), HMIMPF<sub>6</sub> (b), OMIMPF<sub>6</sub> (c), HMIMCl (d), OMIMCl (e), HMIMBr (f), and OMIMBr (g) at 298.15 K and 1 atm.

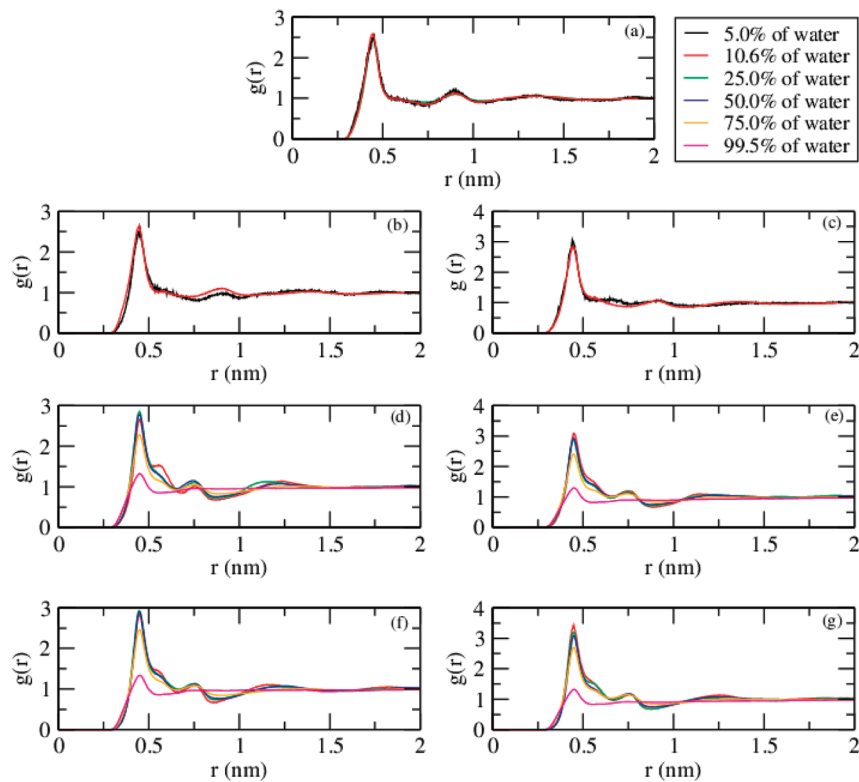


**Figure 6.** Concentration dependence of cation–water RDFs for BMIMPF<sub>6</sub> (a), HMIMPF<sub>6</sub> (b), OMIMPF<sub>6</sub> (c), HMIMCl (d), OMIMCl (e), HMIMBr (f), and OMIMBr (g) at 298.15 K and 1 atm.

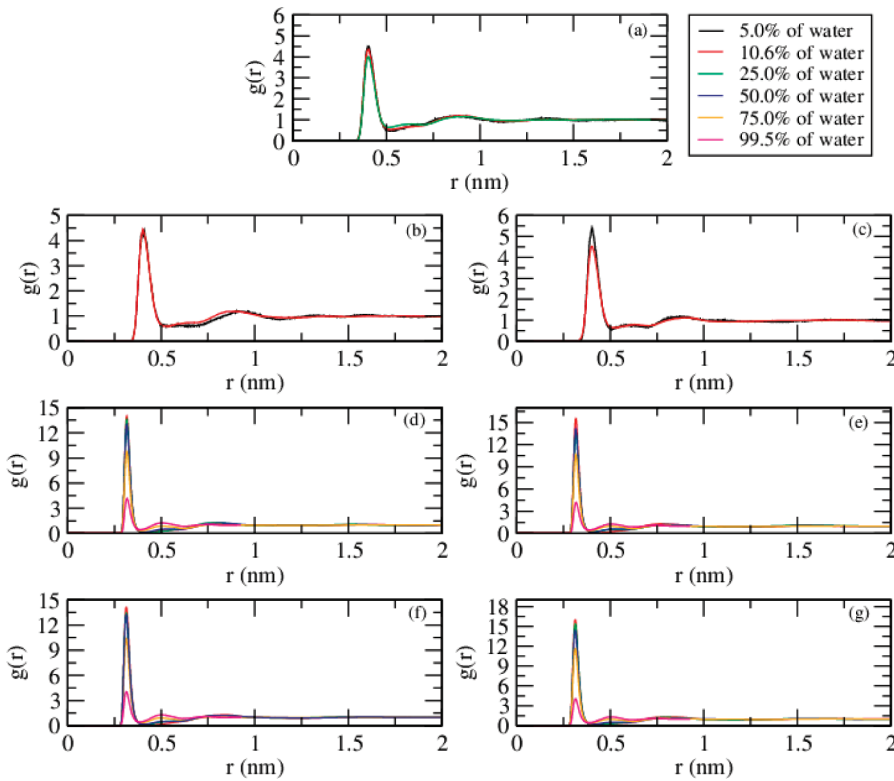


**Figure 7.** Concentration dependence of anion–water RDFs of BMIMPF<sub>6</sub> (a), HMIMPF<sub>6</sub> (b), OMIMPF<sub>6</sub> (c), HMIMCl (d), OMIMCl (e), HMIMBr (f), and OMIMBr (g) at 298.15 K and 1 atm.

this clusterization is much more notable in the case of the hydrophobic anion PF<sub>6</sub><sup>-</sup> (Figure 5a–c), for which the height of the peaks is seen to monotonically decrease with water concentration throughout the entire miscibility regions of the different cationic chain length. This is to be attributed to the fact that the number of water contacts increases slower than the number of water molecules in the bulk itself.<sup>21</sup> Moreover, the height of this first peak of the RDF notably increases with alkyl chain length of the cation, a similar behavior to that reported for BMIMBF<sub>4</sub> and OMIMBF<sub>4</sub> by Feng and Voth in ref 21. The first peaks of the ILs with the hydrophobic PF<sub>6</sub><sup>-</sup> are much higher than those of their halogenated homologues with the same cationic chain length (Figure 5d–g), confirming the role of the hydrophobicity of the cation in the spatial correlation of water in bulk IL mixtures. It is also interesting to compare our results for OMIMPF<sub>6</sub> with that for OMIMBF<sub>4</sub> reported by Feng and Voth in the Figure 2 b of ref 21. The height of the first peak of the RDF for OMIMBF<sub>4</sub> at a water concentration of  $w = 20\%$  is roughly 15, while in our case it is around 33 for  $w = 20\%$ , as expected given the stronger hydrophobicity of the PF<sub>6</sub><sup>-</sup> anion as compared to BF<sub>4</sub><sup>-</sup>. Consequently, we can conclude that water is strongly clusterized in AMIMPF<sub>6</sub> ILs in the very narrow miscibility regions of these hydrophobic compounds and that the increase in the number of cations in the alkyl side chain dramatically affects the structuring of water in the bulk.

The situation is somehow different for the mixtures with halogenated compounds (Figure 5d–g). While in AMIMPF<sub>6</sub> water seems to exhibit no remarkable long-ranged order (no secondary peaks important enough relatively to the first peaks are observed), this is not the case for the ILs with halogen anions. In these cases, we can observe the existence of more marked

long-ranged order, particularly visible in the less studied low water concentration region. The crucial role of the anion in water structure is strongly suggested by these observations, and it is further reinforced comparing the RDFs of HMIMPF<sub>6</sub> and OMIMPF<sub>6</sub> with their hydrophilic homologues with halogenated anions in Figure 5d–g. The heights of the first peaks in the latter cases are less than half their values for the hydrophobic compound. Moreover, as we mentioned previously, while the intensity of the first peak of the w/w RDF for AMIMPF<sub>6</sub> monotonically decreases as the concentration of water increases, until it finally recovers the RDF of pure water, the situation is much richer in the case of the hydrophilic halogen anions. As can be seen in the inset of Figure 5d, an inversion is registered between the heights of this peak for 50% water concentration and 75% water concentration in all the considered ILs, which is indicative of a stronger spatial correlation of water molecules at this percentage of water. This behavior is in agreement with the behavior reported for OMIMBF<sub>4</sub> and OMIMCl by Feng and Voth.<sup>21</sup> This behavior was also reported by Hanke and Lynden-Bell for dMIMCl–water mixtures<sup>16</sup> and by Jiang et al.<sup>14</sup> for OMIMNO<sub>3</sub>, and the latter authors also associated this enhancement of the water–water spatial correlation to the formation of heterogeneous water networks. Moreover, we detected a previously unreported inversion of the first peak of the RDF, which exhibits an inversion at the lowest concentrations analyzed,  $w = 10\%$  and  $w = 25\%$ , highly dependent on the cation and anion nature. Interestingly enough, the inversion is detected in mixtures of the IL with the longest cation chain length (OMIM) for Cl<sup>-</sup> and in HMIM for Br<sup>-</sup>. This behavior suggests some kind of interplay between cation chain length and anion size, but the actual origin of this correlation needs further study.

As stated above, a detailed analysis of the highly diluted water regime was not previously reported for IL–water mixtures, to our knowledge. Thus, we extended our simulations down to a water concentration of  $w = 10\%$  corresponding to 25 molecules of water in our ensemble, and as can be seen in Figures 5d–g, two very interesting features concerning the structure of the water network in the mixture are observed in this regime. First, we observe in Figures 5a–c that relatively weak peaks associated to the second neighbors of the central water molecule are registered around 0.5 nm in AMIMPF<sub>6</sub> for all water concentrations and that the peaks of the third neighbors can be neglected in practice relative to the first ones of these compounds. However, strongly marked second and third peaks are registered at 0.37 and 0.6 nm, respectively, for aqueous mixtures of the halogenated salts of HMIM<sup>+</sup> and OMIM<sup>+</sup> in the low to intermediate water concentration regime (up to  $w = 50\%$ ). Even a fourth peak is registered for the lowest concentration. This reflects once more that water in hydrophilic ILs adopt a less densely packed, more dispersed arrangement of small water clusters coordinated with hydrophilic anions, while in hydrophobic ILs water tends to adopt a highly organized network of large water clusters even at very low concentrations. This effect will also be reflected in the number of w/w hydrogen bonds, as it will be seen. Water molecules tend to be strongly clusterized in dispersed clusters at the lowest concentrations coordinated with hydrophilic anions, and only at high enough concentrations continuous water regions are formed in the bulk mixture. Hence, at the lowest analyzed concentrations, the addition of water molecules reinforces local water clusters leading to an increase of the first peak together with a weakening of longer range spatial correlations between water clusters associated to higher order peaks of the RDF. Moreover, Cl<sup>-</sup> anions seem to perturb more strongly the structure of added water than Br<sup>-</sup>, in agreement with the positions of these anions in the Hoffmeister series, in which Br<sup>-</sup> is two positions above Cl<sup>-</sup>, and so the latter tends to be more strongly hydrated than Br<sup>-</sup> due to the highly localized point charge of the former. In both cases three strongly marked peaks (once again, relatively to the height of the first ones), and a more diffuse fourth one, are visible in the w/w RDF for the lowest water concentrations (10%, 25%), and these peaks are still visible at concentrations as high as 50% (Figures 5d–g). However, in the case of Cl<sup>-</sup> (Figures 5d and 5e), the heights of the peaks and the depth of the valleys are higher than those for Br<sup>-</sup> (Figures 5f and 5g). Moreover, the close proximity of the first and second peaks (less than 0.1 nm) suggests again the effect of the different lengths of the alkyl side chains of the cation on the water shell surrounding it.

Figures 6 and 7 show, respectively, the RDFs of cation–water and anion–water in the studied mixtures. In all the cases shown in Figure 6 one can observe a first peak around 0.45 nm which slightly increases with cationic chain length. Moreover, it is apparent in Figures 6 and 7 that the presence of halogen ions induces a more oscillatory behavior in the RDFs, reflecting once more the more long-ranged order in these cases when compared to those of ILs with the PF<sub>6</sub><sup>-</sup> anion. Particularly, in this latter case, the first and second peaks in the RDFs in Figures 6a–c and 7a–c are separated a distance of ca. 0.5 nm, indicating that throughout the whole miscibility region water weakly hydrates the cationic chain, probably due to the presence of a hydrophobic anion, and prefers to form its own clusters in agreement with our previous interpretation of w/w RDFs. This is certainly not the case for the halogen anions, for which water molecules are less

clusterized and more in contact with the cations, as reflected by the positions and heights of the RDFs in Figures 6d–g. The situation is similar for the anion, being the strongly hydrophobic PF<sub>6</sub><sup>-</sup> (Figures 7a–c) much less hydrated than their halogens counterparts (Figures 7d–g), as reflected both by the height of the first peaks of the RDFs of the halogenated IL–water mixtures, essentially three times higher than in PF<sub>6</sub><sup>-</sup> based water–IL mixtures, and also by the oscillations around the anion at the origin. Water around the hydrophobic PF<sub>6</sub><sup>-</sup> is structured in two hydration layers separated by 0.5 nm, while for the halogens this distance is only about 0.2 nm. Moreover, as can be seen in these representations, this structuring is weakened in all the studied cases as water concentration increases. Besides, the distance from the central anion to the first hydration layer (position of the first peak) is greater for PF<sub>6</sub><sup>-</sup> than for the halogen ions, as expected due to the greater size of the former and its more hydrophobic character.

Thus, from the analysis of the RDFs we can conclude that water tends to clusterize in the cavities of the IL liquids, the distributions of water in the bulk being strongly dependent on the hydrophobicity degree of the cation and, even more strongly, of the anion. The more hydrophobic the anion, the more clusterized water is in the bulk mixture. Very limited hydration is detected for both cations and hydrophobic PF<sub>6</sub><sup>-</sup>, and water interacts more strongly with the halogen anions. The influence of the cation is much weaker. These conclusions are reinforced with the results shown in Figure 8 in which the average number of hydrogen bonds per water molecule is shown for all the analyzed IL–water mixtures. As mentioned previously, according to ref 52 a hydrogen bond is considered to exist if the distance between the tagged hydrogen and the acceptor is smaller than 0.35 nm and the angle of the donor-hydrogen-acceptor bond is below 30° (according to Gromacs criterion, OH and NH groups are regarded as donors, and O and N are considered to be acceptors). Moreover, we have organized the calculated information in the figure to show the effect of the anions on the number of hydrogen bonds, since it is well-known that water molecules are mainly hydrogen-bonded to anions.<sup>18,53</sup> As can be seen, the number of hydrogen bonds per molecule monotonically increases with the amount of water in all of the studied cases, although for the halogenated ILs this increase is notably smaller than for the PF<sub>6</sub><sup>-</sup> throughout all the miscibility region of this IL. In fact, the average number of hydrogen bonds per water molecule in AMIMPF<sub>6</sub>–water mixtures is already 0.15 at 25% water content, while that value is not reached in the halogenated compounds until a concentration ca. 50%. This fact reinforces the picture of a dispersed network formed by small clusters in the case of ILs with hydrophilic anions, and larger clusters in the case of ILs with more hydrophobic ones. These clusters are more similar to bulk water than their homologous in ILs with hydrophilic anions, thus confirming our interpretation of the results for the RDFs mentioned above. No significant difference is detected in w/w hydrogen bonding degree between the two studied halogen ions.

On the other hand, Figure 9 represents the water–cation hydrogen bonding degree for all of the studied cases. As one can see there, the average number of hydrogen bonds per molecule is greater by almost 1 order of magnitude for AMIMPF<sub>6</sub>–water mixtures than for its halogenated counterparts, probably due to repulsive interactions between water molecules and the hydrophobic anion. The value 10<sup>-4</sup> is reached at 25% water content in AMIMPF<sub>6</sub>–water mixtures, while this value is not reached until a water concentration of 50% for the halogenated anions.

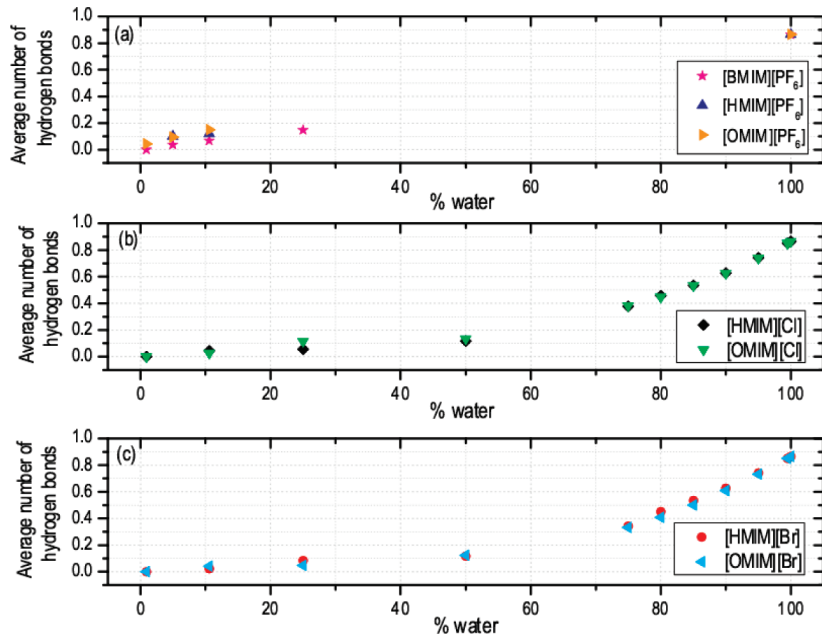


**Figure 8.** Concentration dependence of the average number of water–water hydrogen bonds per water molecule in the mixture.

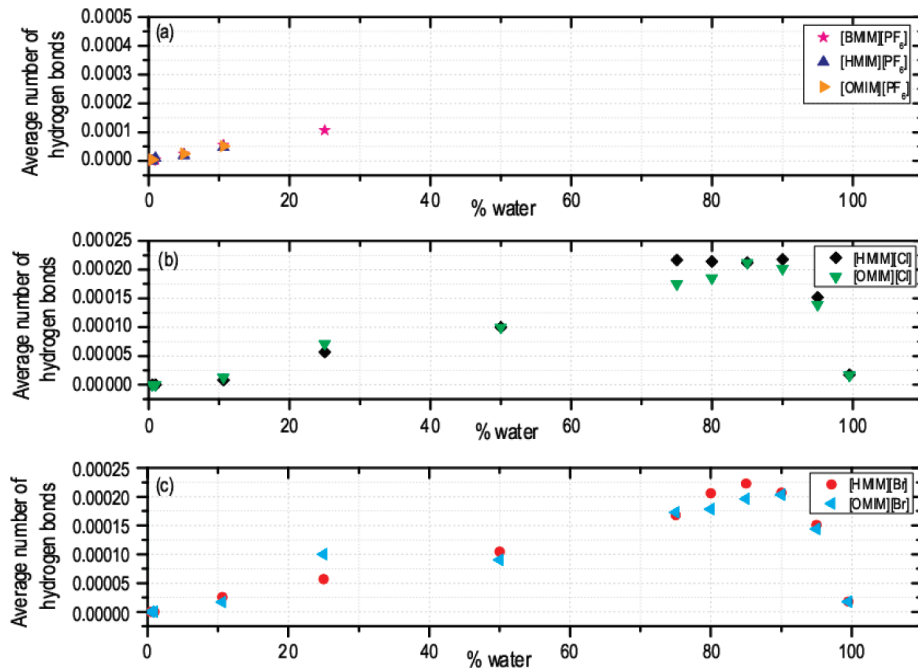


**Figure 9.** Concentration dependence of the average number of cation–water hydrogen bonds per water molecule in the mixture.

Once again, no relevant difference is observed between the two halogens, and only slight differences are observed between alkyl chain lengths, leading the compounds with longer chains to the formation of less hydrogen bonds of cations with water in the high water concentration, as should be expected due to its more hydrophobic nature.

On the other hand, where anion–water is concerned, the hydration numbers of water molecules around the anions were calculated by direct integration of the first peak of the corresponding RDFs up to their first minimum. They show monotonous increases in all cases up to a calculated limiting value of

7.4 for Cl<sup>-</sup> and 7.2 for Br<sup>-</sup>. This value must be compared to an experimental value of 6.<sup>54,55</sup> This overestimation is registered in many other MD force fields, for which values of 7 or even higher have been reported, and similar deviations are reported in the literature.<sup>56</sup>

A pictorial representation of water clustering in these compounds can be observed in Figure 10, where we present a snapshot of the water clusters formed in HMIMPF<sub>6</sub> and HMIMCl at water concentrations of 25% and 75%, respectively. In the former case it is apparent that water molecules present in the mixture are already clusterized even at so low concentrations

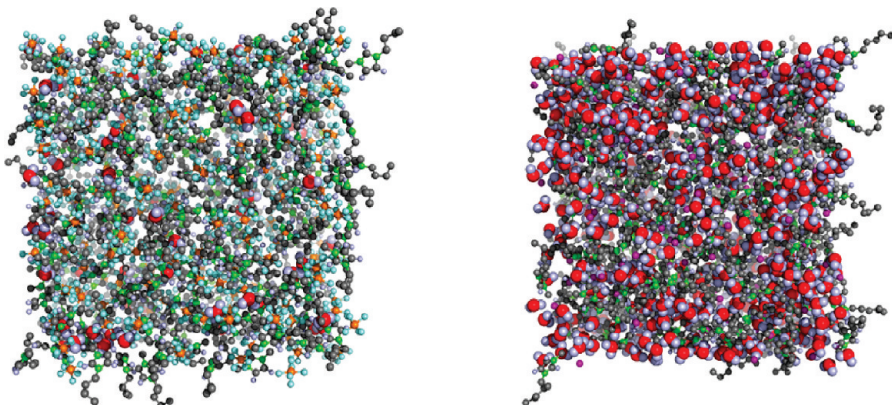


**Figure 10.** Snapshots of (a)  $\text{BMIMPF}_6$ –water mixtures at 25% water concentration (limit of miscibility) and (b)  $\text{HMIMCl}$ –water mixtures at 75% water concentration. Red and gray spheres correspond to oxygen and hydrogen atoms respectively, and for clarity they are augmented.

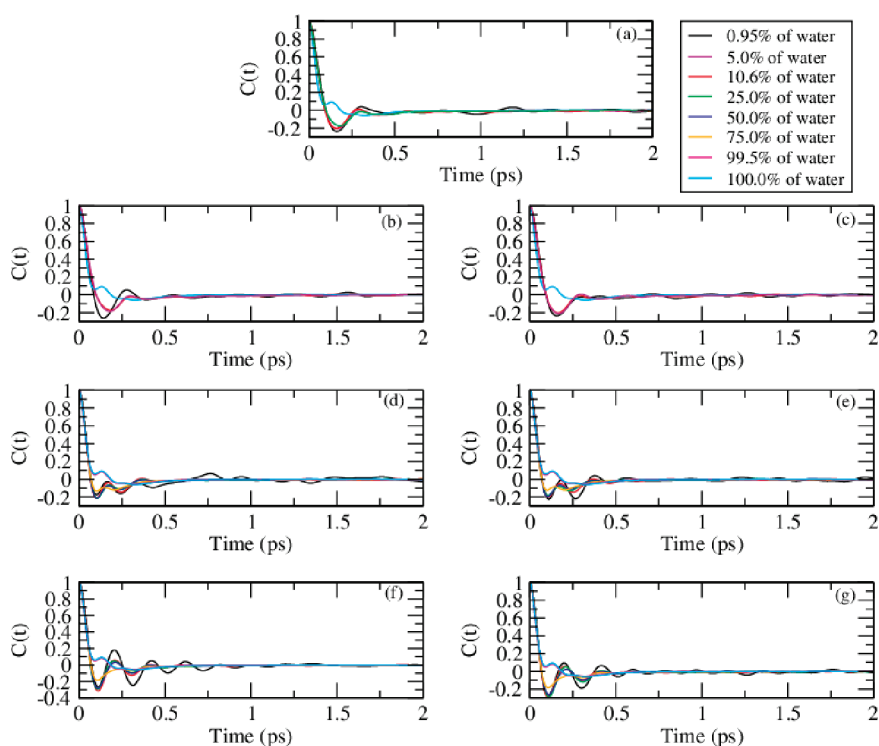


**Figure 11.** Concentration dependence of the water molecules VACF in water mixtures with  $\text{BMIMPF}_6$  (a),  $\text{HMIMPF}_6$  (b),  $\text{OMIMPF}_6$  (c),  $\text{HMIMCl}$  (d),  $\text{OMIMCl}$  (e),  $\text{HMIMBr}$  (f), and  $\text{OMIMBr}$  (g).

(it must be taken into account that a small number of water molecules is included in the simulation), announcing immiscibility by the formation of quasi-continuous aqueous regions inside the mixture. However, in  $\text{HMIMCl}$  small clusters dispersed throughout the mixture are still observed even at such a high water concentration.

We now discuss the results for the dynamical properties of IL–water mixtures, of considerable importance in many processes. In Figure 11 we represent the water VACF, defined as

$$C(t) = \langle \vec{v}(t) \cdot \vec{v}(0) \rangle \quad (3)$$

where  $\vec{v}(t) = \sum_j m_j \vec{v}_j / \sum_j m_j$  is the velocity of the center of mass of the molecule and the scalar product is calculated in the laboratory

frame. As far as we know, these are the first reported simulations for this magnitude in water–IL mixtures. As one can see, the mean collision time of water molecules, as indicated by the first zero of the function, is a little bit greater in the case of  $\text{AMIMPF}_6$  (around 0.1 ps due to the “cage effect”) than those in the halogenated compounds. As we know, water molecules are highly clusterized in these compounds when compared to their halogenated counterparts, and thus water motion in bulk cavities of the mixture is more similar to that in pure water (collision time ca. 0.2 ps). On the other hand, a very limited effect of the chain length on this collision time is registered in all of the studied cases. The correlations are rapidly but nonmonotonically weakened in all mixtures, so within 0.5 ps correlations are no longer present for  $\text{PF}_6^-$  and within 1 ps they are canceled out even for

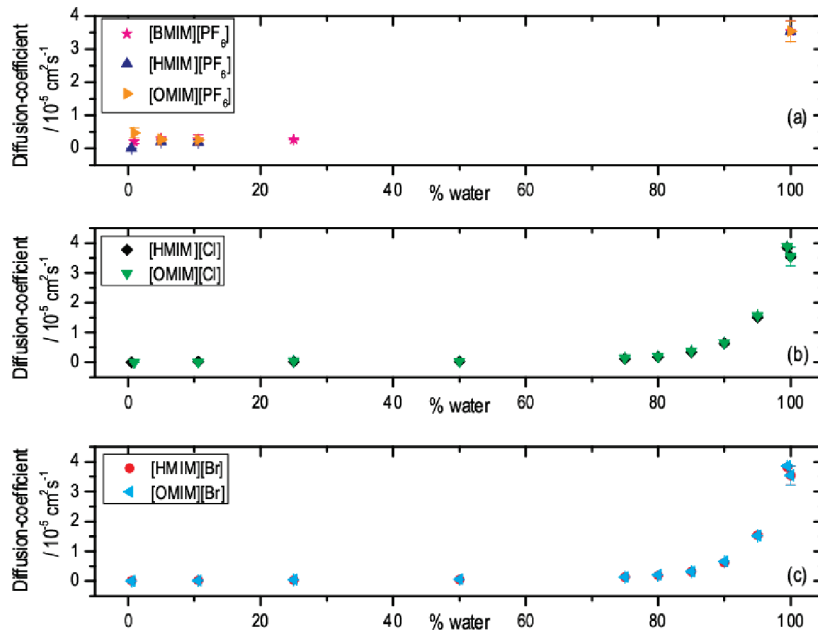


**Figure 12.** Concentration dependence of the diffusion coefficients of water molecules in several mixtures.

the halogenated ILs with the shortest studied chain length ( $\text{HMIM}^+$ ). However, in the case of the halogenated compound, considerable oscillatory behavior of the VACF is registered up to this latter time in all of the studied compounds, in marked contrast with the monotonic weakening registered in pure ILs.<sup>57</sup> This indicates a “rattling” motion of water molecules inside the cages formed by its heavier neighbors<sup>58</sup> that is more marked and relatively more long-lived for the ILs with the shortest chain lengths. Interestingly, this rattling motion is more markedly observed for  $\text{Br}^-$  than for the lightest  $\text{Cl}^-$ , something to be attributable to the fact that this latter anion is more strongly hydrated than the former. Besides, the main effect of water addition is a progressive smoothing out of the VACF until the pure water value is recovered—in agreement to previously reported results.<sup>59,60</sup> Contrarily to what happened with the collision time, an increase in the chain length leads to a less oscillatory behavior of the VACF in the case of the first compounds.

Another important magnitude for the characterization of the single-particle dynamics in dense fluids is the diffusion coefficient. We evaluated this magnitude with the procedure already implemented in the Gromacs package. In Figure 12 we represent the dependence of the self-diffusion coefficients of a water molecule in all the analyzed water–IL mixtures. As it is well-known, two different regimes can be observed for this magnitude: (i) a slow increase in the diffusion coefficients associated to glassy states at low water concentrations, and (ii) a rapid increase at low IL concentrations associated to the formation of the water network. However, as expected, a faster diffusion is observed for AMIM-PF<sub>6</sub> than for the halogenated ILs due to the more hydrophobic character of the PF<sub>6</sub><sup>-</sup> anion.<sup>19</sup> It is also noteworthy that the diffusion coefficients of water molecules in pure ILs are typically 2 orders of magnitude lower than in pure water, in agreement with results previously reported in the literature for imidazolium-based ILs.<sup>19,61</sup> Finally, no significant effects of chain length of the IL cation are detected on the diffusion coefficient of water molecules.

In Figure 13 we represent the MSDs of water molecules and of cation and anion in BMIMPF<sub>6</sub>–water mixtures at 25% water concentration. This magnitude is defined as

$$\langle \Delta |\vec{r}(t)|^2 \rangle = \frac{1}{N} \left\langle \sum_{i=1}^N |\vec{r}_i(t) - \vec{r}_i(0)|^2 \right\rangle \quad (4)$$

where the sum extends over all the molecules present, and the positions of the molecules have been calculated from their centers of mass. Two different regimes can be observed in Figure 13 corresponding to the ballistic motion of the molecules at short times,  $\langle \Delta |\vec{r}(t)|^2 \rangle \propto t^2$ , and a long-time diffusive regime characterized by a Brownian motion,  $\langle \Delta |\vec{r}(t)|^2 \rangle \propto t$ . The intermediate subdiffusive plateaus can be compared to those reported for supercooled liquids near the glass transition (see ref 57 and references therein). We can define the characteristic times of ballistic ( $\tau_b$ ) and diffusive ( $\tau_d$ ) times as the times corresponding to the beginning and the end of the intermediate plateau, that can be estimated as the intersection of the two straight lines corresponding to the plateau and the two lines defining the ballistic and diffusive regimes themselves (see Figure 13). We have calculated in this fashion the evolution of  $\tau_b$  and  $\tau_d$  with water concentration in our mixtures, and the results are represented in Figure 14. As can be seen in this representation, both ballistic and diffusive times decrease with water concentration, so the addition of water provokes a faster transition to the diffusive regime. Moreover, it is noteworthy that  $\tau_b$  is approximately 100 to 1000 times greater than  $\tau_d$ , so the subdiffusive regime extends over hundreds of ps, in accordance with previously reported results.<sup>57</sup> According to del Popolo and Voth,<sup>57</sup> this is indicative of long cage escape times for the water molecules during the intermediate stage, being this subdiffusive dynamics (for which  $\langle \Delta |\vec{r}(t)|^2 \rangle \propto t^\beta$  with  $\beta < 1$ ) characteristic of glass formers. This complex non-Markovian dynamics at intermediate times, which indicates a slow structural relaxation of these liquids, is progressively weakened by the addition of water. We must also mention that these times are shorter for the more hydrophobic cation, and

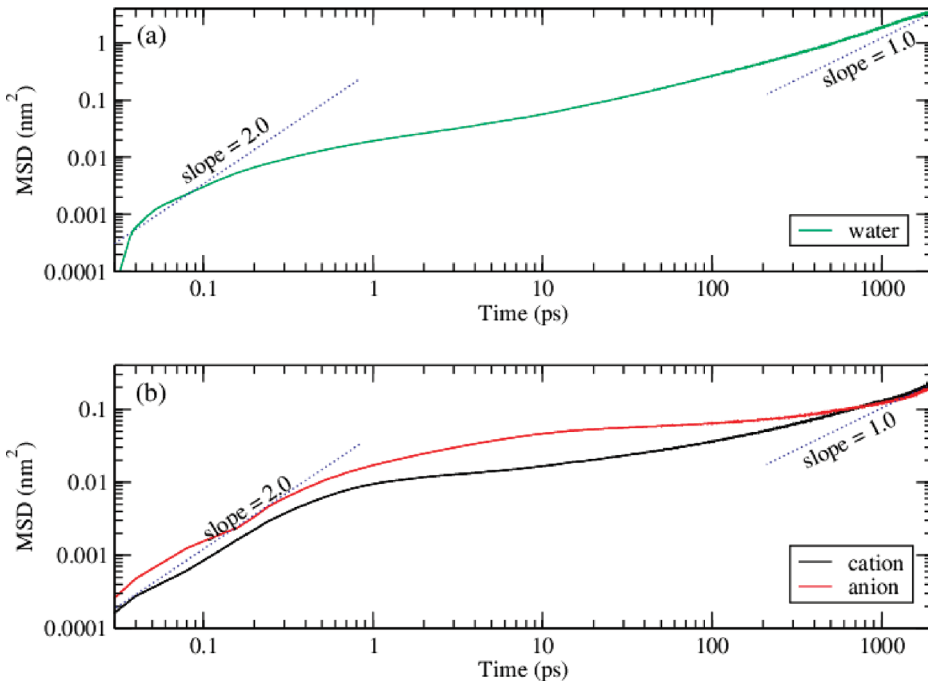


**Figure 13.** Log–log plot of the MSDs of (a) water and (b) cation and anion in a mixture with BMIMPF<sub>6</sub> at 25% water concentration. Dotted lines of slope 1 and 2 have been included to identify the ballistic and diffusive regimes.

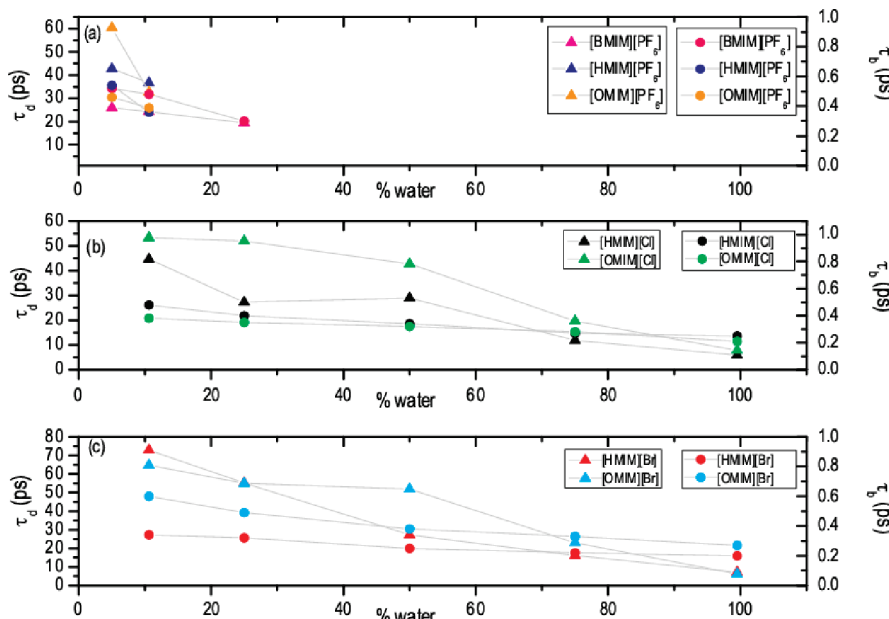


**Figure 14.** Evolution of the ballistic (triangles) and diffusive (circles) characteristic times with water concentration in water-IL mixtures. Lines are guides to the eye.

for the Cl<sup>-</sup> anion in the case of the halogenated ILs, in agreement with our previous observations for the clusterization of water in mixtures with these ILs. According to the exposed above, water is more strongly clusterized following the series PF<sub>6</sub><sup>-</sup> > Cl<sup>-</sup> > Br<sup>-</sup>, so the opposite behavior is expected for the transition time to diffusive motion typical of pure water. Finally, let us point out that these times seem to be maximized for HMIM<sup>+</sup> in all of the studied cases, but the precision of our estimations does not allow a more accurate prediction at this stage.

#### 4. CONCLUSIONS

We have presented systematic computer simulations of the structure and dynamics of water mixtures with imidazolium-based ILs of different hydrophobicities (including the highly hydrophobic anion PF<sub>6</sub><sup>-</sup> throughout its entire miscibility regime), and we have analyzed the influence of both anion and cation hydrophobicity degrees, and of water concentration on the structural and dynamic properties. Particularly, we have analyzed RDFs, coordination numbers, and average degree of

hydrogen bonding of the ionic and molecular species present in the bulk mixtures. We have seen that water tends to clusterize in the cavities of the IL, being the water structuring in the bulk strongly dependent on the hydrophobicity degree of the cation and, even more strongly, of the anion, that leads to greater clusterization of water molecules in the bulk mixtures as its hydrophobic character increases. The average number of hydrogen bonds per molecule is greater by almost 1 order of magnitude for AMIMPF<sub>6</sub>—water mixtures than for its halogenated counterparts, probably due to repulsive interactions between water molecules and the hydrophobic anion. On the other hand, the analysis of the velocity autocorrelation function of water molecules revealed that the correlations cancel out faster for water-IL mixtures with more hydrophobic anions, and that rattling motion of water molecules is registered in the cavities of the halogenated ILs, this motion being more intense when the anion is less hydrated. Two different regimes were observed for the diffusion coefficients of water molecules in IL—water mixtures: (i) a slow increase in the diffusion coefficients associated to glassy states at low water concentrations, and (ii) a rapid increase at low IL concentrations associated to the formation of the water network. Faster diffusion was observed for AMIMPF<sub>6</sub> than for the halogenated ILs due to the more hydrophobic character of the PF<sub>6</sub><sup>-</sup> anion. Finally, complex non-Markovian dynamics at intermediate times associated to slow structural relaxation of the mixtures are observed. Ballistic and diffusive times were respectively defined as the upper and lower bounds of the ballistic region at short times and the diffusive regime at long times, after the molecule has undergone many collisions in the bulk. These times were shown to be shorter for more hydrophobic cation, and for the Cl<sup>-</sup> anion in the case of the halogenated ILs, as determined by the degree of clusterization of water in mixtures with these ILs. A comprehensive study of both single-particle and collective dynamics of IL—water mixtures and of mixtures of ILs with other molecular liquids are now in progress and will be presented in a forthcoming paper.

## AUTHOR INFORMATION

### Corresponding Author

\*E-mail address: luismiguel.varela@usc.es.

## ACKNOWLEDGMENT

The authors wish to thank the financial support of Spanish “Ministerio de Educación y Ciencia” under the research projects FIS2007-66823-C02-0, FIS2007-66823-C02-02, and FIS2008-04894/FIS and also the funding of Xunta de Galicia through the research projects of references 10-PXI-103-294 PR and 10-PXIB-206-294 PR. Moreover, this work has been funded by the Directorate General for R+D+i of the Xunta de Galicia (INCITE09E2R206033ES). All of these research projects are partially supported by FEDER funds. J. Carrete and T. Méndez-Morales thank the Spanish ministry of Education for their FPU grants.

## REFERENCES

- (1) Welton, T. *Chem. Rev. (Washington, DC, U.S.)* **1999**, *99*, 2071–2084.
- (2) Wilkes, J. *Green Chem.* **2002**, *4*, 73–80.
- (3) Wilkes, J. S.; Zaworotko, M. J. *J. Chem. Soc., Chem. Commun.* **1992**, *1992*, 965–967.
- (4) Hagiwara, R.; Ito, Y. *J. Fluorine Chem.* **2000**, *105*, 221–227.
- (5) Earle, M. J.; Seddon, K. R. *Pure Appl. Chem.* **2000**, *72*, 1391–1398.
- (6) Earle, M. J.; Esperança, J. M. S. S.; Gilea, M. A.; Lopes, J. N. C.; Rebelo, L. P. N.; Magee, J. W.; Seddon, K. R.; Widgren, J. A. *Nature (London, U.K.)* **2006**, *439*, 831–834.
- (7) Wakai, C.; Oleinikova, A.; Ott, M.; Weingärtner, H. *J. Phys. Chem. B* **2005**, *109*, 17028–17030.
- (8) Carrete, J.; García, M.; Rodríguez, J. R.; Cabeza, O.; Varela, L. M. *Fluid Phase Equilib.* **2011**, *301*, 118–122.
- (9) Cuadrado-Prado, S.; Domínguez-Pérez, M.; Rilo, E.; García-Garabal, S.; Segade, L.; Franjo, C.; Cabeza, O. *Fluid Phase Equilib.* **2009**, *278*, 36–40.
- (10) Bowers, J.; Butts, C. P.; Martin, P. J.; Vergara-Gutierrez, M. C. *Langmuir* **2004**, *20*, 2191–2198.
- (11) Malham, I. B.; Letellier, P.; Turmine, M. *J. Phys. Chem. B* **2006**, *110*, 14212–14214.
- (12) Firestone, M. A.; Dzielawa, J. A.; Zapol, P.; Curtiss, L. A.; Seifert, S.; Dietz, M. L. *Langmuir* **2002**, *18*, 7258–7260.
- (13) Antonietti, M.; Kuang, D.; Smarsly, B.; Zhou, Y. *Angew. Chem., Int. Ed.* **2004**, *43*, 4988–4992.
- (14) Jiang, W.; Wang, Y.; Voth, G. A. *J. Phys. Chem. B* **2007**, *111*, 4812–4818.
- (15) Kelkar, M.; Shi, W.; Maginn, E. J. *Ind. Eng. Chem. Res.* **2008**, *47*, 9115–9126.
- (16) Hanke, C. G.; Lynden-Bell, R. M. *J. Phys. Chem. B* **2003**, *107*, 10873–10878.
- (17) Canongia-Lopes, J. N.; Costa Gomes, M. F.; Padua, A. A. H. *J. Phys. Chem. B* **2006**, *110*, 16816–16818.
- (18) Spickermann, C.; Thar, J.; Lehmann, S. B. C.; Zahn, S.; Hunger, J.; Buchner, R.; Hunt, P. A.; Welton, T.; Kirchner, B. *J. Chem. Phys.* **2008**, *129*, 104505–104517.
- (19) Porter, A.; Liem, S. Y.; Popelier, L. A. *Phys. Chem. Chem. Phys.* **2008**, *10*, 4240–4248.
- (20) Urahata, S. M.; Ribeiro, M. C. C. *J. Chem. Phys.* **2004**, *120*, 1855–1863.
- (21) Feng, S.; Voth, G. A. *Fluid Phase Equilib.* **2010**, *294*, 148–156.
- (22) Chevrot, G.; Schurhammer, R.; Wipff, G. *Phys. Chem. Chem. Phys.* **2006**, *8*, 4166–4174.
- (23) Inoue, G.; Shimoyama, Y.; Su, F.; Takada, S.; Iwai, Y.; Arai, Y. *J. Chem. Eng. Data* **2007**, *S2*, 98–101.
- (24) Freire, M. G.; Santos, L. M. N. B. F.; Fernandes, A. M.; Coutinho, J. A. P.; Marrucho, I. M. *Fluid Phase Equilib.* **2007**, *261*, 449–454.
- (25) Wong, D. S. H.; Chen, J. P.; Chang, J. M.; Chou, C. H. *Fluid Phase Equilib.* **2002**, *194*–197, 1089–1095.
- (26) Margulis, C. J.; Stern, H. A.; Berne, B. J. *J. Phys. Chem. B* **2002**, *106*, 12017–12021.
- (27) Spoel, D. V. D.; Lindahl, E.; Hess, B.; Buuren, A. R. V.; Apol, E.; Meulenhoff, P. J.; Tieleman, D. P.; Sijbers, A. L. T. M.; Feenstra, K. A.; Drunen, R. V.; Berendsen, H. J. C. *Gromacs User Manual version 3.2*; <http://www.Gromacs.org>, 2005.
- (28) Spoel, D. V. D.; Lindahl, E.; Hess, B.; Buuren, A. R. V.; Apol, E.; Meulenhoff, P. J.; Tieleman, D. P.; Sijbers, A. L. T. M.; Feenstra, K. A.; Drunen, R. V.; Berendsen, H. J. C. *Gromacs User Manual version 4.0*; <http://www.Gromacs.org>, 2005.
- (29) Scott, W. R. P.; Hünenberger, P. H.; Tironi, I. G.; Mark, A. E.; Billeter, S. R.; Fennem, J.; Torda, A. E.; Huber, T.; Krüger, P.; Gunsteren, W. F. V. *J. Phys. Chem. A* **1999**, *103*, 3596–3607.
- (30) Bayly, C. I.; Cieplak, P.; Cornell, W.; Kollman, P. A. *J. Phys. Chem.* **1993**, *97*, 10269–10280.
- (31) Berendsen, H. J. C.; Grigera, J. R.; Straatsma, T. P. *J. Phys. Chem.* **1987**, *91*, 6269–6271.
- (32) Darden, T.; York, D.; Pedersen, L. *J. Chem. Phys.* **1993**, *98*, 10089–10094.
- (33) Essmann, U.; Perera, L.; Berkowitz, M. L.; Darden, T.; Lee, H.; Pedersen, L. G. *J. Chem. Phys.* **1995**, *103*, 8577–8593.
- (34) Jorgensen, W. L.; Madura, J. D. *J. Am. Chem. Soc.* **1983**, *105*, 1407–1413.

- (35) Mahoney, M. W.; Jorgensen, W. L. *J. Chem. Phys.* **2000**, *112*, 8910–8922.
- (36) Cornell, W. D.; Cieplak, P.; Bayly, C. I.; Gould, I. R.; Merz, K. M.; Ferguson, D. M.; Spellmeyer, D. C.; Fox, T.; Caldwell, J. W.; Kollman, P. A. *J. Am. Chem. Soc.* **1995**, *117*, 5179–5197.
- (37) Jorgensen, W. L.; Maxwell, D. S.; Tirado-Rives, J. *J. Am. Chem. Soc.* **1996**, *118*, 11225–11236.
- (38) Zielkiewicz, J. *J. Chem. Phys.* **2005**, *123*, 104501–104506.
- (39) Klähn, M.; Stüber, C.; Seduraman, A.; Wu, P. *J. Phys. Chem. B* **2010**, *114*, 2856–2868.
- (40) Head-Gordon, T.; Johnson, M. E. *Proc. Natl. Acad. Sci. U.S.A.* **2006**, *103*, 7973–7977.
- (41) Berendsen, H. J. C.; Postma, J. P. M.; Gunsteren, W. F. V.; Dinola, A.; Haak, J. R. *J. Chem. Phys.* **1984**, *81*, 3684–3690.
- (42) Morrow, T. I.; Maginn, E. J. *J. Phys. Chem. B* **2002**, *106*, 12807–12813.
- (43) Bowron, D. T.; D'Agostino, C.; Gladden, L. F.; Hardacre, C.; Holbrey, J. D.; Lagunas, M. C.; McGregor, J.; Mantle, M. D.; Mullan, C. L.; Youngs, T. G. A. *J. Phys. Chem. B* **2010**, *114*, 7760–7768.
- (44) Bahe, L. W. *J. Phys. Chem.* **1972**, *76*, 1062–1071.
- (45) Varela, L. M.; García, M.; Sarmiento, F.; Attwood, D.; Mosquera, V. *J. Chem. Phys.* **1997**, *107*, 6415–6419.
- (46) Souto, J.; Alemany, M. M. G.; Gallego, L. J.; González, L. E.; González, D. *J. Phys. Rev. B* **2010**, *81*, 134201–134215.
- (47) Alavi, S.; Thompson, D. L. *J. Chem. Phys.* **2005**, *122*, 154704–154715.
- (48) Liu, Z.; Wu, X.; Wang, W. *Phys. Chem. Chem. Phys.* **2006**, *8*, 1096–1104.
- (49) Liu, Z.; Huang, S.; Wang, W. *J. Phys. Chem. B* **2004**, *108*, 12978–12989.
- (50) Micaelo, N. M.; Baptista, A. M.; Soares, C. M. *J. Phys. Chem. B* **2006**, *110*, 14444–14451.
- (51) Hardacre, C.; McMath, S. E. J.; Nieuwenhuyzen, M.; Bowron, D. T.; Soper, A. K. *J. Phys.: Condens. Matter* **2003**, *15*, S159–S166.
- (52) Hess, B.; Kutzner, C.; Spoel, D. V. D.; Lindhal, E. *J. Chem. Theory Comput.* **2008**, *4* (3), 435–447.
- (53) Köddermann, T.; Wertz, C.; Heintz, A.; Ludwig, R. *Angew. Chem., Int. Ed.* **2006**, *45*, 3697–3702.
- (54) Stuart, S. J.; Berne, B. J. *J. Phys. Chem.* **1996**, *100*, 11934–11943.
- (55) Raugei, S.; Klein, M. L. *J. Chem. Phys.* **2002**, *116*, 196–202.
- (56) Ohtaki, H. *Chem. Rev.* **1993**, *93*, 1157–1204.
- (57) Del Popolo, M. G.; Voth, G. A. *J. Phys. Chem. B* **2004**, *108*, 1744–1752.
- (58) Hansen, J.-P.; MacDonald, I. R. *Theory of Simple Liquids*; Academic Press: Oxford, 1986.
- (59) Harsányi, I.; Pusztai, L.; Soetens, J.-C.; Bopp, P. A. *J. Mol. Liq.* **2006**, *129*, 80–85.
- (60) Sokol, M.; Dawid, A.; Dendzik, Z.; Gburski, Z. *J. Mol. Struct.* **2004**, *704*, 341–345.
- (61) Sieffert, N.; Wipff, G. *J. Phys. Chem. B* **2005**, *109*, 18964–18973.